JOURNAL OF THERMOPHYSICS AND HEAT TRANSFER
Vol. 16, No. 3, July–September 2002

Single-Bubble Dynamics During Pool Boiling Under Low Gravity Conditions

D. M. Qiu* and V. K. Dhir†
University of California, Los Angeles, Los Angeles, California 90095
and
D. Chao,‡ M. M. Hasan,‡ E. Neumann,§ G. Yee,¶ and A. Birchenough¶
NASA John H. Glenn Research Center at Lewis Field, Cleveland, Ohio 44135

Results of an experimental study on growth and detachment mechanisms of a single bubble on a heated surface conducted during the parabola flights of the KC-135 aircraft are described. An artificial cylindrical cavity 10 μm in diameter was etched in the center of a silicon wafer. The wafer was heated on the back side, and the wall superheat was controlled. Degassed distilled water was used as the test liquid. Bubble growth time, bubble size and shape from nucleation to liftoff were measured under subcooled and saturation conditions at system pressures varying from 0.101 to 0.115 MPa. The wall superheats were varied from 2.5 to 8.0°C. Significantly larger bubble diameters and longer bubble growth periods than those at Earth normal gravity were measured. Bubble diameters as large as 20 mm at liftoff were observed as opposed to about 2.5 mm at Earth normal gravity. Consistent with results of numerical simulations, it is found that for the same wall superheat and liquid subcooling the bubble liftoff diameter can be approximately related to the gravity level through the relation $D_d \propto g^{-0.5}$ and the growth period as $t_g \propto g^{-1.05}$. The effect of wall superheat and liquid subcooling on bubble liftoff diameter is found to be small. However, the growth periods are found to be very sensitive to liquid subcooling at a given wall superheat. Small accelerations along the heater surface can lead to sliding motion of the bubble prior to liftoff. At the same gravitational acceleration the liftoff diameter of sliding bubbles is smaller than that of nonsliding bubbles.

Nomenclature

D	=	bubble diameter, m
g	=	gravity, m/s^2
H	=	height, m
h_{fg}	=	latent heat of vaporization, J/kg
k	=	thermal conductivity, W/(m · K)
T_s	=	saturation temperature, °C
t	=	time, s
U	=	velocity, m/s
V	=	velocity, m/s
β	=	contact angle, deg
ΔT_{sub}	=	liquid subcooling, $\Delta T_{\text{sub}} = T_s - T_{\text{liquid}}$, °C
ΔT_w	=	wall superheat, $\Delta T_w = T_{\text{wall}} - T_s$, °C
$\Delta\rho$	=	density difference between liquid and vapor, kg/m^3
δ_T	=	thermal-layer thickness
ρ	=	density, kg/m^3
σ	=	surface tension, N/m

Subscripts

a	=	advancing
b	=	bubble base
d	=	detachment (liftoff)
e	=	Earth normal
g	=	growth
l	=	liquid
m	=	moment when bubble starts to lift off
r	=	receding
s	=	at the moment when bubble starts to slide
v	=	vapor
x	=	direction parallel to the heater surface and along the plane
y	=	direction parallel to the heater surface and across the plane
z	=	direction normal to the heater surface

Received 27 August 2001; revision received 22 February 2002; accepted for publication 5 April 2002.

*Postdoctoral Fellow; currently Engineer, Velocys, Inc., Columbus, OH 43017.
†Professor, Department of Mechanical and Aerospace Engineering; vdhir@seas.ucla.edu.
‡Scientist, Microgravity Science Division.
§Engineer, Facilities and Test Engineering Division.
¶Engineer, Microgravity Science Division.

Introduction

BOILING is known as a highly efficient mode of heat transfer. It is employed in component cooling and in various energy conversion systems. For space applications boiling is the heat-transfer mode of choice because the size of the components can be significantly reduced for a given power rating. For any space mission the size and in turn the weight of the component plays an important role in the economics of the mission. Applications of boiling heat transfer in space can be found in such areas as thermal management, fluid handling and control, and power systems. For space power systems based on the Rankine cycle (a representative power cycle), the key issues that need to be addressed are the magnitude of boiling heat-transfer coefficient and the critical heat flux under low-gravity conditions.

The investigations of boiling heat transfer for space applications impose unique constraints in terms of the number of experiments that can be conducted under microgravity conditions, the duration of the experiments, and the expense and the difficulties involved in performing the experiments. Thus, for space applications it is even more important that a better understanding of the boiling mechanisms be developed and the performance features of the experiments be explored in advance. The low-gravity environment of the KC-135 aircraft provides a less expensive means to accomplish these tasks.

Under microgravity conditions the early data of Keshock and Siegel[1] and Siegel and Keshock[2] on bubble growth and heat transfer show that the effect of reduced gravity is to reduce the buoyancy and inertia forces acting on a bubble. As a result, under reduced gravity bubbles grow larger and stay longer on the heater surface. This in turn leads to merger of bubbles on the heater surface and existence of conditions similar to those for fully developed nucleate boiling. Thus, they concluded that under microgravity conditions partial nucleate boiling region can be very short or nonexistent.

Ervin et al.[3] and Ervin and Merte[4] have studied transient nucleate boiling on a gold film sputtered on a quartz plate of an area 19×38 mm^2 by using a 5-s drop tower (10^{-5} g_e) at NASA Glenn Research Center. In the experiments R113 was used as the test liquid. It was found that the time or temperature for initiation of nucleate boiling was greater for liquid at near saturation temperature than that for a subcooled liquid. They also noted the occurrence of energetic boiling at relatively low heat fluxes. The energetic boiling in which vapor mass rapidly covered the heater was postulated to be associated with an instability at the wrinkled vapor–liquid interface. Subsequently, Merte[5] and Lee and Merte[6] have reported results of pool boiling experiments conducted in the space shuttle for a surface similar to that used in the drop tower tests. Subcooled boiling during long periods of microgravity was found to be unstable. The surface was found to dryout and rewet at higher surface heat flux. At 11.5°C subcooling it was observed that after a period of growth of small bubbles and their coalescence, a larger bubble formed, which stayed above the surface. The larger bubble acted as a reservoir sucking and removing the smaller bubbles from the surface. Average heat-transfer coefficients during the dryout and rewetting periods were found to be about the same. The nucleate boiling heat fluxes were higher than those obtained on a similar surface at Earth normal gravity g_e conditions. It was concluded that subcooling has negligible influence on the steady-state microgravity heat-transfer coefficient. The effect of Marangoni convection (thermocapillary flow) on the heat transfer was considered to be reduced at microgravity conditions.

Straub et al.[7] and Straub[8] have conducted a series of nucleate boiling experiments using thin platinum wires and gold-coated flat plates as heaters at low-gravity conditions in the flights of ballistic rocket and KC-135. In the experiments R12 and R113 were used as test liquids at saturation and subcooled conditions. The results from the thin wires showed that at low gravity and low heat fluxes the heat-transfer coefficients were slightly higher or were the same as those at Earth normal gravity conditions for both saturated and subcooled liquids. Quasi-steady state was reached in these experiments. The translating movement of vapor along the wire was described. Large number of nucleation sites and relatively stronger Marangoni convection were believed to be the mechanism of heat transfer at low gravity. For the flat-plate heater with R12 as the test liquid, boiling curves similar to those at g_e were obtained when the liquid was saturated. With R113, rapid bubble growth and large bubbles ($D \geq 2$ cm) were observed during the TEXUS ballistic rocket flight at gravity level of 10^{-4} g_e. However, no bubbles were seen to lift off from the heater surface, and neither temperature nor heat flux reached a steady state. For subcooled R113 and R12 a reduction in heat-transfer coefficient of up to 50% in comparison to that at g_e was obtained. It was observed that larger bubbles occupied the surface, and at their edges many smaller bubbles formed, coalesced, and fed the larger ones.

Ohta et al.[9] have reported results of bubble behavior during boiling of ethanol on a glass surface under the microgravity environment of the ballistic rocket. They observed formation of a large vapor bubble with many primary bubbles at the base. Local dryout was noted to have occurred underneath primary bubbles; however, a relatively thick liquid layer was seen to remain between the coalesced bubble base and the test surface. From their experiments in KC-135, Kim et al.[10] have noted that the coalesced large bubble oscillates while supported by many smaller primary and secondary bubbles.

Recently, Ma and Chung[11] experimentally studied single-bubble dynamics in flow boiling of FC72 at terrestrial gravity and reduced gravity in a 1-s drop tower. Pyrex glass substrate coated with thin gold film with an effective heating area 1×1 mm^2 was used to create a single bubble in the subcooled liquid, $\Delta T_{sub} = 26$°C, for liquid velocity varying from 6.5 to 30 cm/s. It was observed that at reduced gravity the bubble diameter at departure from the nucleation site (horizontally) is larger than that at terrestrial gravity. After the departure the bubble slides along the heater surface and shrinks as a result of the lower wall temperature outside the heating area. However, no liftoff of the bubble from the heater surface in reduced gravity conditions is described.

From the preceding description it appears that results from studies conducted until now are inconclusive. Questions remain on the conditions of nucleation initiation, the stability of nucleate boiling, the roles of liquid microlayer underneath the stationary and translating bubble, the reasons for equivalence of magnitudes of heat-transfer coefficients at normal-gravity and low-gravity conditions, and the forces driving bubbles off from or sliding along the surface and on the overall physics that underlies the phenomena. As such, there is no mechanistic model that describes the observed physical behavior and the dependence of nucleate boiling heat flux on wall superheat.

When the dependence of cavity site density on wall superheat is known (true for designed surface with artificial cavities), the prediction of heat flux requires a knowledge of interfacial area per cavity, interfacial heat flux, and heat transfer on the unpopulated area of the heater. Size of bubbles at breakoff, bubble release frequency (growth period + waiting time), and the number of bubble release sites influence the time and area averaged heat transfer and also determine the vapor removal rate.

As a first step in developing and validating a mechanistic model for prediction of nucleate boiling heat transfer, in this work the complete process of nucleation inception to bubble growth to liftoff for a single bubble formed at a well-defined and controllable nucleation site is studied.

Description of Experiments

A well defined nucleation site is formed in the middle of a silicon wafer. Heating of the surface is provided by strain gage heaters attached to the wafer surface underneath. The power to the heaters is adjusted to maintain a desired temperature. Visual observations of bubble dynamics are made through a video camera.

Experimental Setup

The experimental apparatus for the KC-135 flights is schematically shown in Fig. 1. The system configuration is the same as that used by Merte[5] in the flight experiments in the space shuttle. It consists of a test chamber ($D = 15$ cm, $H = 10$ cm), a bellow, and a nitrogen (N_2) chamber. Three glass windows are installed on the walls of the test chamber for the visual observations. For the control of the system, pressure transducers are installed in the test chamber

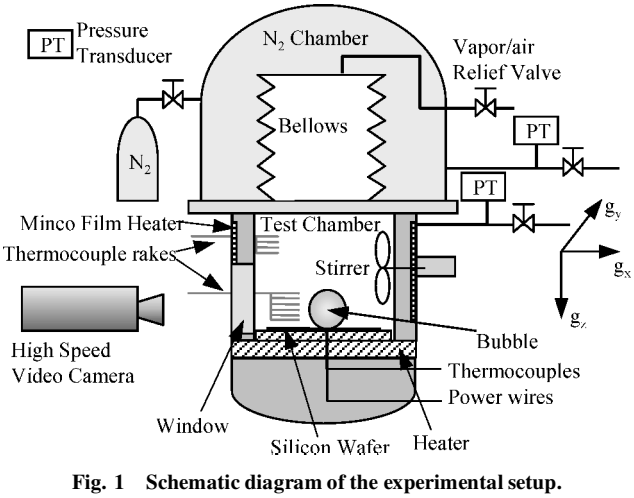

Fig. 1 Schematic diagram of the experimental setup.

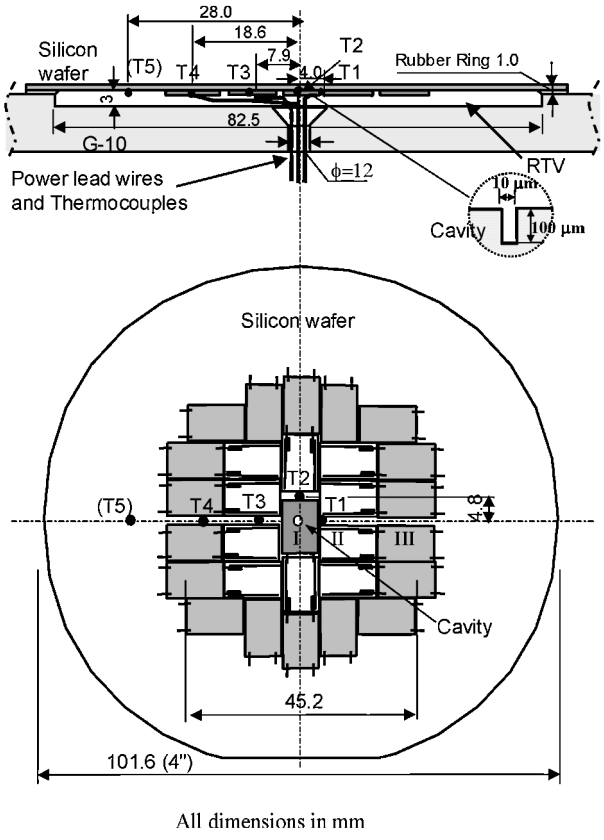

Fig. 2 Silicon wafer instrumented with strain gauge heaters and thermocouples.

and N_2 chamber, respectively. The test surface for studying nucleate boiling is installed at the bottom of the test chamber (Fig. 2). In the vicinity of the heater surface, a rake of six thermocouples is installed in the liquid pool to measure the temperature in the thermal boundary layer, while another thermistor rake is placed in the upper portion of the chamber to measure the bulk liquid temperature.

Distilled, filtered, and degassed water was used as the test liquid. Two video cameras were installed to record the boiling processes. One of them operates at 250 frames/s and provides digitalized images with increased magnification. The second one is used for an overall view of the boiling process. The liquid temperature and pressure in the chamber were controlled according to the set points established by the operator on board. A three-component accelerometer is installed on the frame on which the setup is mounted.

Heater with a Designed Nucleation Site

A polished silicon wafer 101.6 mm in diameter and 1 mm in thickness was used as the test surface for the nucleate boiling experiments. From the manufacturer's specification the roughness of the bare polished wafer is less than 0.5 nm. A cylindrical cavity of 10 μm in diameter and 100 μm in depth was etched in the wafer center via the deep reactive ion etching technique.

At the back of the silicon wafer, the foil-like strain gauge heating elements were bonded. Each of the elements has an effective heating area of 6.5×6.5 mm^2 and was separately wired with the wires taken out from the hole in the base made from Phenolic Garolite Grade 10 (G-10). The heating elements are grouped in different regions. In each group a thermocouple is directly attached to the wafer. The heater surface temperatures in different regions are then separately controlled through a multichannel feedback control system. As such, the surface superheat can be maintained constant during an experimental run and be automatically changed to the desired set point. Figure 2 shows the location of heaters and thermocouples on the silicon wafer. The wafer is cast with RTV, -silicon rubber, on the G-10 base. The base in turn is mounted in the test chamber.

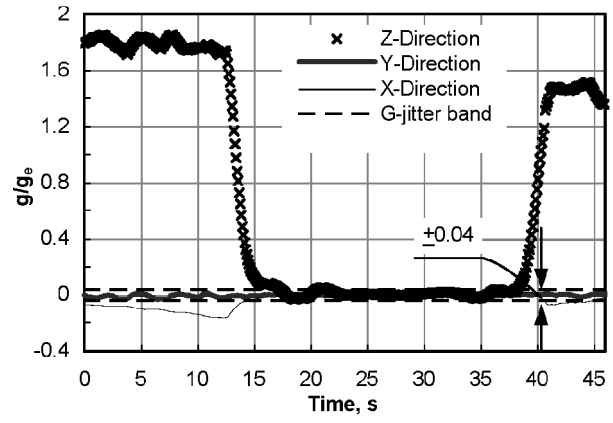

Fig. 3 Typical acceleration excursion during a parabolic flight.

Experimental Procedure

Before each flight the boiling experiments were conducted in the laboratory to ensure the existence of nucleate boiling on the cavity formed in silicon heater and to examine the operation readiness of the system at Earth normal gravity. Before the plane took off, the cavity was activated by energizing the heating elements underneath the cavity. The wall superheat at the cavity area was gradually increased until the inception of nucleation occurred. For saturated water the wall superheat at nucleation inception was generally 12–17°C. However, after activation the wall superheat could be reduced 4–5°C while maintaining the cavity active.

Figure 3 shows a typical gravity level imposed on the test apparatus during the parabolic flights of KC-135. During the low-gravity period, the gravity level in the direction z normal to the heater surface basically varied within a range of $g_z \approx \pm 0.04\ g_e$ (g-jitter), with the accidental increases up to 0.065 g_e. The period of this low-gravity condition was about 20 s. In between the parabolic flights the bulk liquid was maintained at a uniform temperature via a stirrer and the film heaters on the chamber wall. The system pressure was set to 0.115 MPa. Before entering the low-gravity condition, the stirrer was switched off, and the pressure was decreased to the value corresponding to the desired subcooling or saturation temperature. Once the gravity g_z normal to the heater started to decrease below the level $\sim 1.8\ g_e$ (see Fig. 3), the surface temperature of the silicon wafer was set to the desired superheat. The control system simultaneously turned on the video camera and recorded pressure, temperature, and acceleration data. Because of the high conductivity of the silicon wafer (157 W/m · K) and the generally small difference in the actual wall superheat before low-gravity period and the desired value during the experiments, the lag time of the response in the wall superheat is small; it took less than 4 s to reach the set point of wall superheat for the largest superheat difference. This value was determined by examining the recorded temperature histories at low-gravity and from the parameter adjustment of the proportional integral differential controller during the first several flights. In the low-gravity condition ($g_z = \pm 0.04\ g_e$) the surface superheat, water subcooling, and the system pressure were maintained nearly constant.

The uncertainty in the gravity level measurement is mainly from the synchronization uncertainty between the accelerometer recording and the high-speed video recording while gravity level g_z varied within $\pm 0.04\ g_e$ as a result of the flight conditions. An examination using laser pulse with signal recorded in the data files and pulse light displayed in the view of the video recording shows a mismatch in time of less than 0.5 s, which corresponds to the maximum uncertainty of $\pm 0.002\ g_e$ in the level of gravity, g_z, normal to the test surface. The uncertainty in the pressure measurement is ± 0.0034 MPa. This value yields an uncertainty in evaluating the saturation temperature of ± 0.1°C. The temperature measurements of the heater surface and the liquid have an accuracy of 0.1°C. The uncertainty in the evaluation of bubble size is ± 0.05 mm, which is determined from the clarity of the images and the error in contour tracking, whereas the uncertainty in the measurement of contact angle mainly depends on the image clarity and is estimated to be ± 1 deg.

Results and Discussion

Single-Bubble Dynamics at Earth Normal Gravity

Partial nucleate boiling experiments with single bubbles were first conducted at Earth normal gravity using a similar test surface in order to establish a benchmark for scaling the effect of gravity on the bubble dynamics. A charge-coupled device video camera operating at 1200 frames/s was employed. This speed is higher than that in low-gravity tests in view of the short growth periods of vapor bubble on ground.

Figure 4 shows a typical history of equivalent diameter of a single bubble and that of its base at the heater surface during one growth cycle in nearly saturated water at Earth normal gravity. The equivalent bubble diameter is defined as the diameter of a sphere having the same volume as the bubble. Bubble is seen to lift off when its equivalent diameter is about 2.5 mm. It takes about 40 ms for the bubble to attain this size. During the period of bubble growth, the bubble base also expands, reaches a maximum value, stays at the maximum value for some time, and then shrinks as the bubble begins to detach. Maximum bubble base diameter is observed to be between 30–40% of the bubble diameter at liftoff.

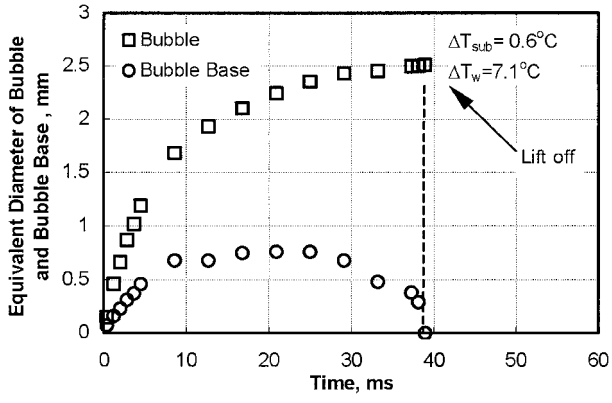

Fig. 4 Growth rate of single bubble at Earth normal gravity.

As the contact angle is one of the important parameters that determine the bubble liftoff diameter, the static contact angle was measured by taking photograph of a water droplet on the heater surface in air. It was found to be about 55 deg. The dynamic contact angle during the evolution of the bubble in water was also measured. The receding contact angle β_r during the expansion of bubble base was found to be in the range of 45–51 deg while the advancing contact angle β_a during the liftoff phase varied between 55 and 61 deg. These values of contact angle are about the same as those measured by Ramanujapu and Dhir[12] at Earth normal gravity for the same solid-liquid combination.

Figure 5 shows the effect of wall superheat on the bubble liftoff diameter (Fig. 5a) and growth period (Fig. 5b). Each data point is the mean value of more than 5 growth-liftoff cycles of single bubbles so that a variability band can be drawn indicating the maximum, minimum, and average of measured values. Figure 5a shows a very weak effect of wall superheat on the bubble liftoff diameter ranging from 2.3 to 2.6 mm for wall superheats from 5.8 to 9.0°C in nearly saturated water at one atmospheric pressure. In contrast, the growth period is significantly affected by the wall superheat as seen in Fig. 5b. The larger the superheat the shorter is the growth period.

The effect of liquid subcooling on bubble diameter at liftoff and growth period is shown in Figs. 6a and 6b, respectively. As the subcooling is increased from 0 to about 3°C while keeping

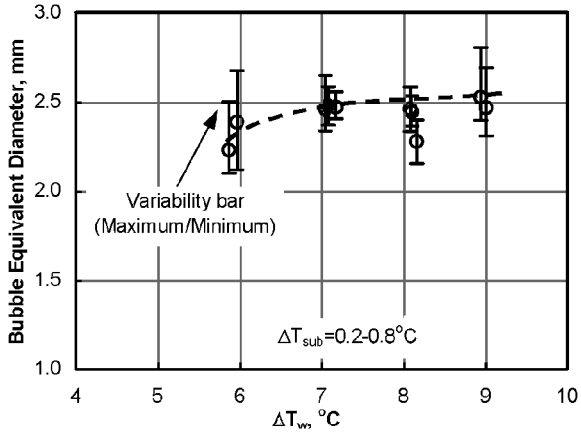

a) Effect of wall superheat on bubble liftoff diameter

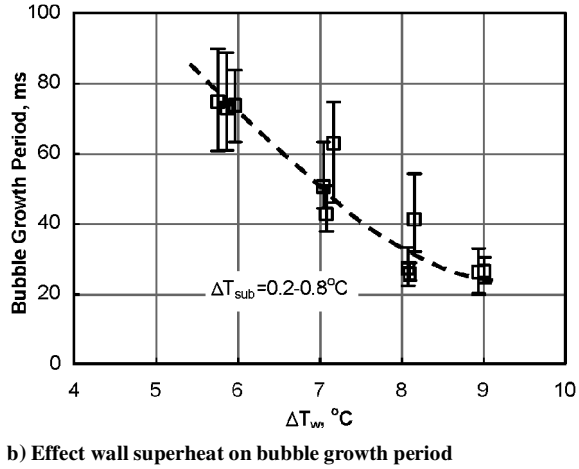

b) Effect wall superheat on bubble growth period

Fig. 5 Effect of wall superheat on bubble liftoff diameter and growth period at 1 g_e.

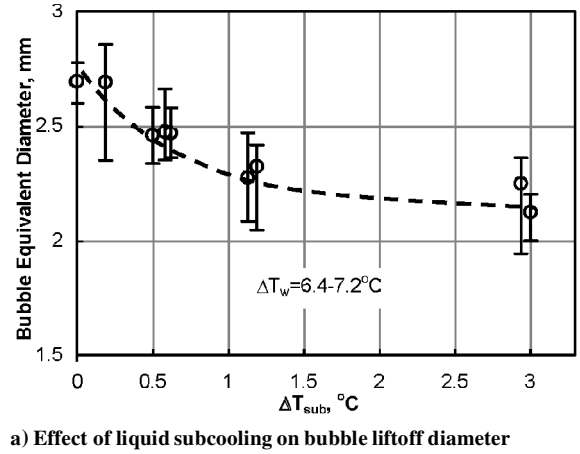

a) Effect of liquid subcooling on bubble liftoff diameter

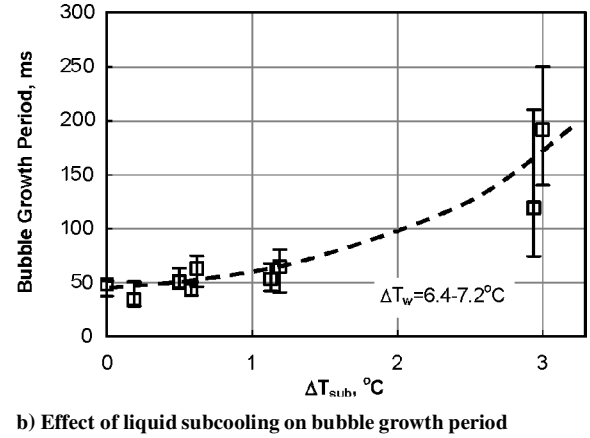

b) Effect of liquid subcooling on bubble growth period

Fig. 6 Effect of liquid subcooling on bubble liftoff diameter and growth period at 1 g_e.

the wall superheat nearly constant, the bubble liftoff diameter decreases (Fig. 6a). At higher liquid subcoolings oscillations in the bubble growth were observed from the high-speed video recordings: The bubble height and diameter alternatively increase and decrease until liftoff, which is usually accompanied by a large amplitude oscillation. These data are not included in Fig. 6a. The bubble growth period is seen to increase monotonically with liquid subcooling.

Single-Bubble Dynamics Under Low-Gravity Conditions

Boiling Process and Bubble Shape

Figure 7 shows the selected photographs of a complete cycle of bubble growth with the nucleation occurring at the designed cavity. The superheat ΔT_w was 4.2°C, and the liquid subcooling ΔT_{sub} was 0.3°C at a system pressure of 0.101 MPa. It is seen that the bubble has a shape of a truncated sphere during the growth period prior to liftoff. The bubble base is seen to first increase, reach a maximum (Fig. 7c), and then decrease to zero. At the moment of bubble liftoff, the video image showed a point-like contact of the bubble with the surface.

Contact angles during the evolution of the bubble were also measured. The receding contact angle (bubble-base expansion phase) was found to vary between 32–45 deg, whereas during the detachment phase (advancing angle) it was about 45–60 deg. These values are slightly smaller than those at Earth normal gravity.

Bubble-base diameter and bubble height are plotted in Fig. 8a. The data were obtained from the video pictures such as those shown in Fig. 7. Initially, as the bubble height increases bubble-base diameter also increases. However, after reaching a maximum value the bubble-base diameter shrinks as bubble starts to detach from the heater surface and as bubble height increases rapidly. Maximum bubble-base diameter is about 40% of the bubble height. This behavior is similar to that observed at Earth normal gravity. Because a microlayer forms underneath the bubble, an increase in bubble-base diameter reflects a corresponding increase in the contribution of evaporation from the microlayer.

Similar data for wall superheat ΔT_w of 2.5°C and liquid subcooling ΔT_{sub} of 0.2°C are plotted in Fig. 8b. It is found that with reduced superheat and in turn reduced transfer of heat from the vapor-liquid interface of the bubble the growth of the bubble slows down. As a result, the increase in bubble-base diameter is also gradual. Maximum bubble-base diameter is again about 35% of the bubble height just prior to liftoff.

Effects of Wall Superheat and Liquid Subcooling on Bubble Growth

Figure 9 shows equivalent bubble diameter as a function of time for wall superheats of 6.5, 5.5, and 3.7°C. The variations of the wall superheat during bubble growth were within ±0.15°C. With increase in wall superheat, the bubble growth rate increases, and bubble growth period decreases under low-gravity environment of the KC-135 aircraft. This behavior is similar to that at Earth normal gravity and is reflective of the increase in heat-transfer rate through the microlayer and the vapor bubble boundary as wall superheat is increased. The bubble diameter at liftoff is found to be about the same for the three superheats when the gravity level at liftoff varied between 0.035 and 0.04 g_e.

Cyclic growth and liftoff of bubbles in the low-gravity environment of KC-135 aircraft is shown in Fig. 10 for a wall superheat of 5.5°C. From cycle to cycle some variations in bubble growth period and bubble diameter at liftoff are seen for $g_z/g_e \approx 0.04$. In the temperature-controlled experiments the waiting time between bubble liftoff and inception of the succeeding bubbles is negligible in comparison to growth period.

Effect of liquid subcooling on bubble growth is shown in Fig. 11. The data were obtained when g_z/g_e varied between 0.03 and 0.04 and for a wall superheat of 3.5°C and for liquid subcoolings of 0, 0.2, and 0.3°C at a system pressure of 0.101 MPa. As discussed earlier, with increased liquid subcooling the bubble growth rate decreases, and bubble growth period increases. However, the effect on bubble diameter at liftoff is small if any. With a subcooling of just 0.3°C, the bubble growth period is increased from 9 to 15 s. The increase is large in comparison to that observed in experiments at Earth normal gravity. The probable cause for this is that under low-gravity conditions larger surface area of the bubble is exposed to subcooled liquid. Thus, in low-gravity experiments it is very important to know the liquid pool temperature precisely as slight subcooling can lead to large variation in bubble growth period without affecting the bubble diameter at liftoff.

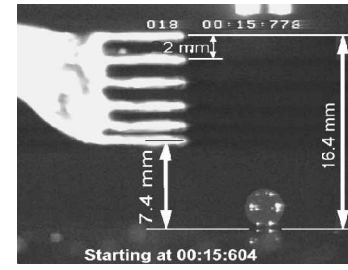

a) $t = 0.17$ s

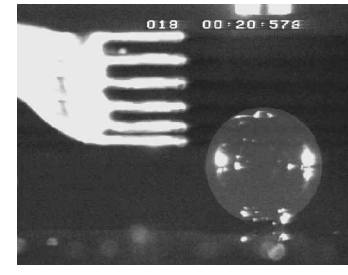

b) $t = 4.97$ s

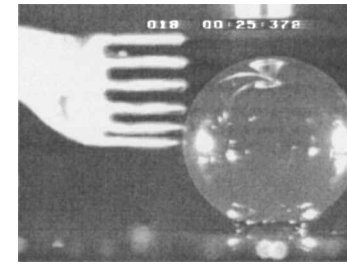

c) $t = 9.77$ s (maximal base)

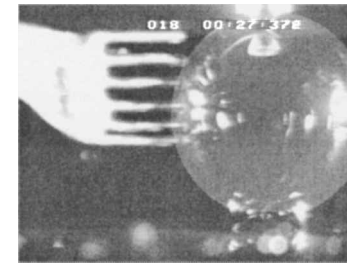

d) $t = 11.77$ s

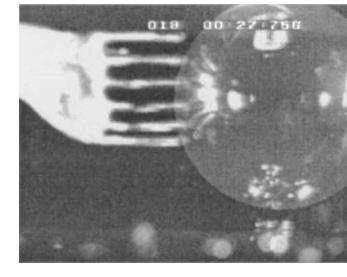

e) $t = 12.15$ (lifting off)

Fig. 7 Selected pictures of the single bubble during a growth-liftoff cycle (inception of nucleation at $t = 0$ s), $\Delta T_{\text{sub}} = 0.3$°C, $\Delta T_w = 4.2$°C, and $g_z \approx 0.02 g_e$.

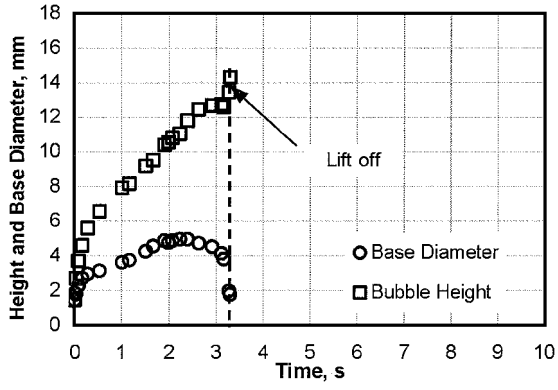

a) $\Delta T_{sub} = 0.0°\,C$, $\Delta T_w = 5.5°\,C$, and $g_z \approx 0.040\, g_e$

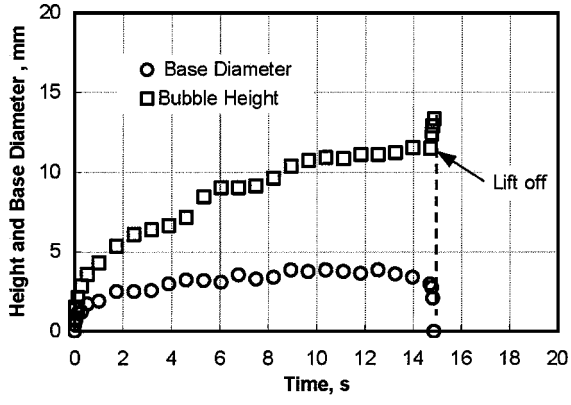

b) $\Delta T_{sub} = 0.2°\,C$, $\Delta T_w = 2.5°\,C$, and $g_z \approx 0.045\, g_e$

Fig. 8 Bubble height and base diameter as function of time at low gravity.

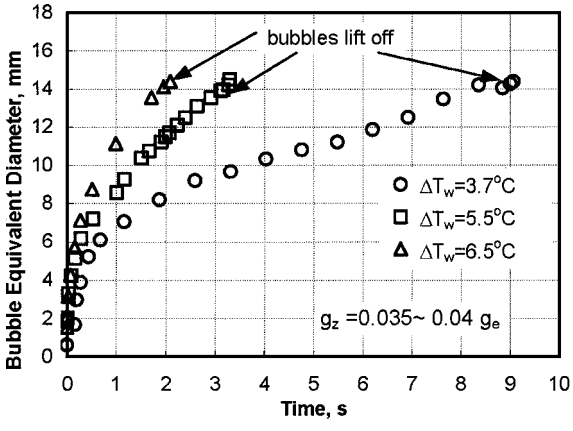

Fig. 9 Bubble growth at different wall superheats in saturated water $g_z = 0.035 \sim 0.04\, g_e$.

Comparison with the Predictions from Numerical Simulations

The measured diameter of the bubble as a function of time in the low-gravity environment of KC-135 is compared in Fig. 12 with the prediction from the numerical simulations as described by Son et al.,[13] Singh and Dhir,[14] and Singh[15] for the saturated liquid and when the liquid has a subcooling of 0.4°C.

In both cases the agreement between the data and model prediction is generally good. The model not only correctly predicts the bubble diameter at liftoff but also the bubble growth period. In both cases the bubble diameter at liftoff is about the same, but with slight subcooling and lower superheat the growth period is increased by a factor of three. Some deviations between prediction and data are seen for the subcooled case during the middle of the growth period of the bubble. Some possible reasons for this difference are the directional changes in the acceleration normal to the heater and in local liquid subcooling that occur during the course of the parabola flight of KC-135 aircraft.

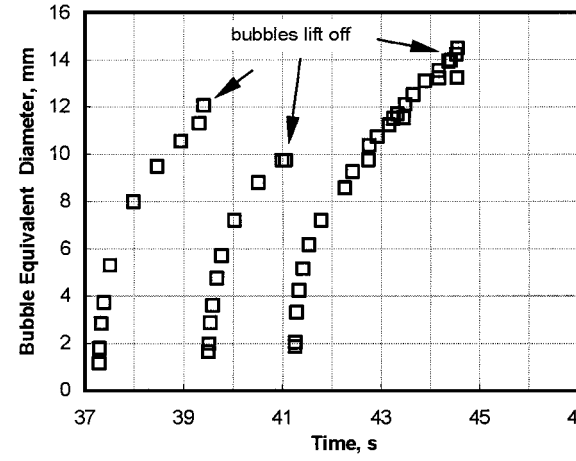

Fig. 10 Multiple cycles of bubble growth at $\Delta T_w = 5.5°\,C$ in saturated water $g_z \approx 0.04\, g_e$.

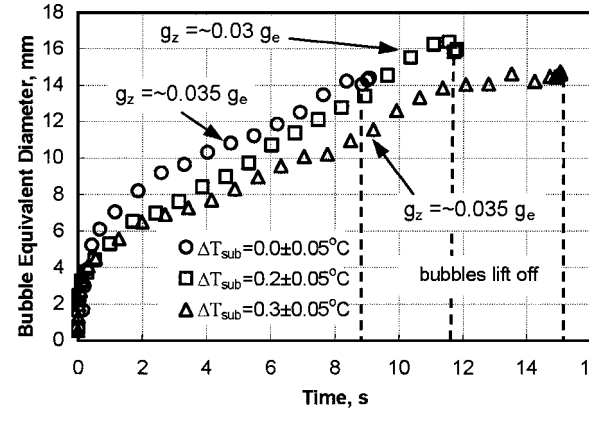

Fig. 11 Bubble growth at slightly different subcoolings for $\Delta T_w = 3.5 \pm 0.2°\,C$.

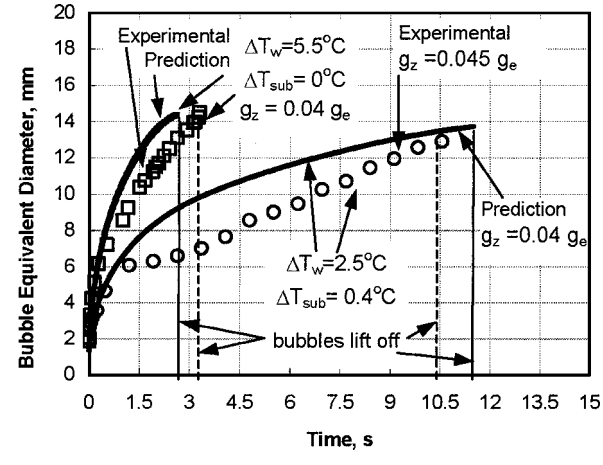

Fig. 12 Comparisons of measured bubble diameter and numerical prediction in saturated water and in subcooled water at low gravity.

Scaling of Effect of Gravity on Bubble Liftoff Diameter and Growth Period

As discussed by Singh and Dhir,[14] under slow bubble growth inertial force is not important, and the bubble diameter at liftoff is approximately given by the balance between surface tension and buoyancy forces:

$$\sigma D_d (\text{surface tension}) \propto \Delta\rho g D_d^3 (\text{buoyancy})$$

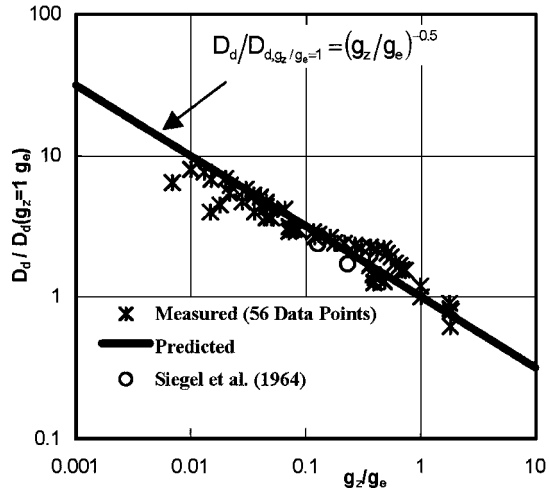

Fig. 13 Bubble diameter at liftoff as a function of the gravity level.

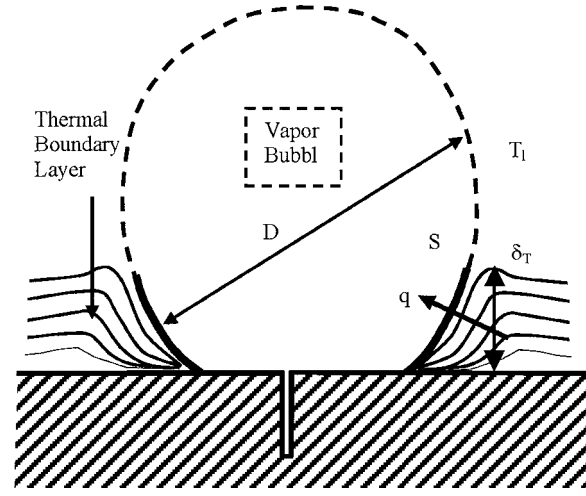

Fig. 14 Simple thermal analysis of growth period of a thermally controlled bubble.

If the same liquid and test heater material combination is used at the Earth normal gravity and at the low-gravity environment and the system pressure is the same so that the contact angle, surface tension, and fluid properties do not change, the bubble liftoff diameter can be written as

$$D_d \propto \left(1/\sqrt{g}\right), \qquad D_d/D_{d(g_z/g_e=1)} = (g_z/g_e)^{-\frac{1}{2}} \tag{1}$$

Although during the parabola flights the level of acceleration was reduced in all directions, the gravity level in the direction normal to the test surface was the largest in most cases, and the gravity components in the plane of the surface were negligible. As such, bubble liftoff from the surface was determined primarily by the acceleration normal to the heater surface. In Fig. 13 the ratio of the bubble diameters at any gravity level to that at $g_z/g_e = 1$ is plotted as a function of gravity level. The gravity level used is that which existed just prior to bubble liftoff rather than that existed during the lifetime of the bubble. In normalization the Earth gravity data obtained at about the same wall superheat and liquid subcooling as the low gravity data were used (for details of data, see Qiu et al.[16]). The ratio of the bubble diameters at partial gravity ($g_z/g_e \approx 0.35$) and at high gravity ($g_z/g_e \approx 1.8$) obtained during the KC-135 flights are also included. It is seen that for $10^{-2} \leq g_z/g_e \leq 1.8$ the observed bubble diameters at liftoff are in general agreement with Eq. (1). As an example at $g_z/g_e = 10^{-2}$, bubble diameter at liftoff is 10 times as large as that at normal gravity or bubble grows to about 25 mm before liftoff. Similarly, in the microgravity environment of the space shuttle ($g_z/g_e = 10^{-4}$) single bubbles can be expected to grow to about 28 cm in diameter before liftoff. This is in agreement with the predictions from direct numerical simulations.[14]

For a thermally controlled bubble growth the effect of gravity on its growth period can be approximately scaled through a simple thermal consideration as schematically depicted in Fig. 14. For saturated liquid the energy required to create a bubble of equivalent diameter D_d is approximately $\rho_v h_{fg}(4\pi D_d^3/3)$. Neglecting the contribution from microlayer, which can be of the order of 20% as obtained from direct numerical simulations,[13] this energy is transferred from the superheated liquid in the thermal boundary layer (macrolayer) surrounding the bubble and is given by

$$[k_l(T_w - T_s)/\delta_T]\pi D_d \cdot \delta_T \cdot t_g \tag{2}$$

In obtaining the energy transferred from the macrolayer, it is assumed that the thermal layer surrounds only the lower portion of the bubble, and the average heat flux at the interface is the same as at the wall. The former assumption is generally incorrect at bubble inception. However, during most of the bubble life the thermal layer is much thinner than the bubble diameter. Equating the energy required for the bubble growth with the energy supplied from the macrolayer, we obtain

$$\rho_v h_{fg}\left(4\pi D_d^3/3\right) \propto k_l \Delta T_w \pi D_d t_g \tag{3}$$

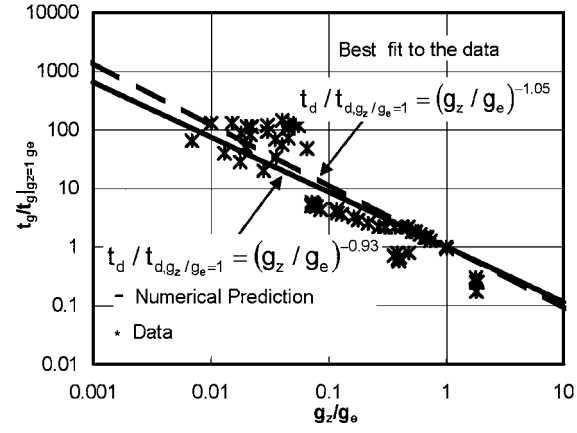

Fig. 15 Bubble growth time before liftoff as a function of the gravity level.

$$t_g \propto D_d^2 \tag{4}$$

Substituting for D_d from Eq. (1), the effect of gravity on bubble growth period is scaled as

$$t_g \propto (1/g_z) = g_z^{-1} \tag{5}$$

In Fig. 15 the single bubble growth period at low gravity normalized by those at Earth normal gravity under the same experimental conditions are plotted, again, as a function of normalized gravity level. The best fit of the data (broken line) suggests a scaling of the effect of gravity as

$$t_g/t_{g(g_z/g_e=1)} = (g_z/g_e)^{-1.05} \tag{6}$$

The solid line is the relation

$$t_g/t_{g(g_z/g_e=1)} = (g_z/g_e)^{-0.93} \tag{7}$$

obtained from the results of direct numerical simulations.[14] It is seen that the experimental results of bubble growth periods are in fair agreement with those predicted from the simple order of magnitude analysis and the numerical simulation. The numerical simulations include the contribution of microlayer as well. The growth period can be approximately scaled as $\sim g^{-1}$, despite the relatively larger scatter in the data. The scatter results from the fact that growth period is more sensitive to wall superheat and liquid subcooling in comparison to the bubble diameter at liftoff. Even at Earth normal gravity the magnitude of scatter in the growth period data is larger

(Figs. 5b and 6b). As such, the normalization using the data at Earth normal gravity introduces even larger scatter.

Sliding of Bubbles and Effect of Horizontal Acceleration

The results just discussed were obtained for the experimental conditions in which the gravity normal to the heater surface was dominant, that is, g_z was significantly larger than g_x and g_y. However, during several of the KC-135 flights the accelerations along the test surface had magnitudes comparable to that normal to the surface during the bubble growth period. In those cases the bubbles prematurely started to slide along the surface before liftoff. This sliding motion of bubbles is not caused by thermo-capillary convection contribution, which is negligible when heat fluxes are small and liquid is saturated. Figure 16 shows photographs at different stages of sliding motion of the bubbles. It is seen that the bubble has an asymmetric shape relative to the center of the bubble base and moves off from the cavity toward the right side. This observation suggests that the force needed for the bubbles to begin sliding along the test surface can be smaller than that needed for bubbles to lift off from a nucleation site. Prior to beginning of sliding motion, the bubble growth was symmetrical with the axis passing through the cavity and is similar to the case when gravity level normal to the test surface dominates. From the data for 20 bubble cycles with sliding motion, it is found that in all of the cases bubble diameters D_s at the moment the bubbles begin to slide fall into a range of 3–5 mm and the magnitude of horizontal accelerations $g_{xy} = (g_x^2 + g_y^2)^{1/2}$ are close to or larger than 0.01 g_e, whereas the gravity normal to the surface g_z at this moment is far smaller than the gravity that is needed to lift the bubble off from the surface according to Eq. (1). As is shown in Fig. 17d at the initial time of the bubble life (<0.1 s), the horizontal acceleration g_x (solid line) is several times larger than the gravity normal to the heater surface g_z (circle symbol) so that the bubble departed from the cavity by sliding in the horizontal direction without liftoff from the surface.

Figures 17a and 17b show the bubble sliding velocity in x direction and the corresponding bubble-base diameter as a function of time. The velocity is measured at the center of the bubble base. It is seen that starting from zero velocity at the initial bubble growth time the bubble velocity first rapidly increases to a peak value (~16 mm/s) and thereafter decreases, while the bubble diameter and bubble-base diameter continue to increase at the same time. After the bubble base reaches the maximum size, the sliding velocity is found to increase again. At the same time the bubble continues to grow so that the gravitational force acting in the bubble sliding direction increases via the horizontal acceleration. After the bubble base starts to shrink prior to liftoff, the bubble velocity again increases more rapidly to 21 mm/s at the liftoff moment.

As the bubble slides on the surface, it is difficult to ascertain from the photographs whether a thin liquid film separates the solid from vapor bubble base or not. The presence of such a thin layer could alter the interfacial tension between solid and vapor and in turn the contact angle. However, no evidence for this could be found from the measured contact angles.

Because of the velocity gradient, a sliding bubble in liquid pool experiences the shear force all around the vapor-liquid interface. This causes additional lift force acting on the sliding bubble and in turn the liftoff of sliding bubbles at a smaller diameter than the bubbles that detach normal to the surface directly from the nucleation site at the same g_z level as shown in Fig. 18. Similar

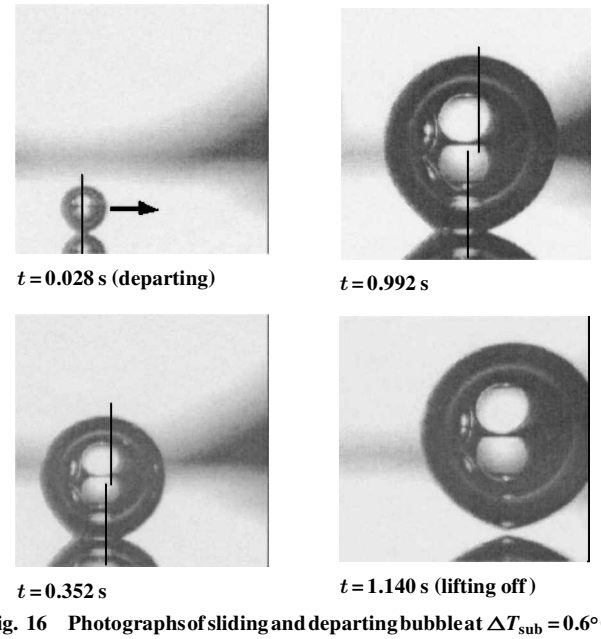

Fig. 16 Photographs of sliding and departing bubble at $\Delta T_{sub} = 0.6°C$, $\Delta T_w = 5.0°C$, $g_z = 0.021\ g_e$, $g_x = -0.009\ g_e$, and $g_y = -0.005\ g_e$.

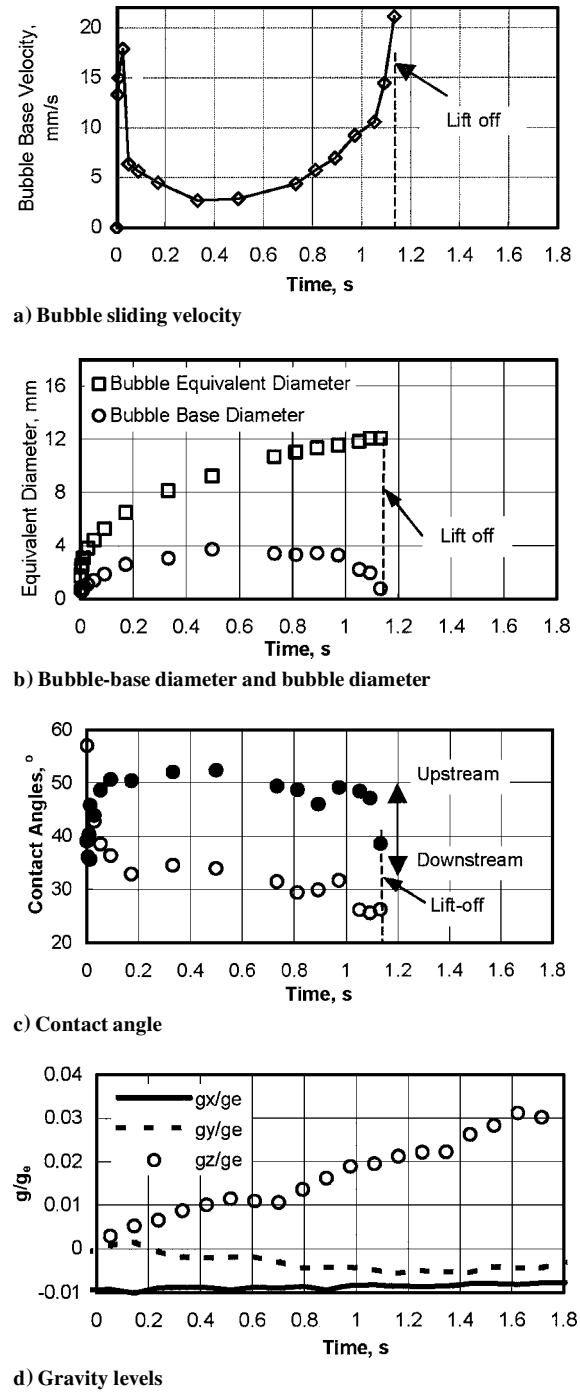

Fig. 17 History of bubble sliding and growth when g_z and g_x are comparable for the same bubble as that in Fig. 16.

Table 1 Comparison of the forces acting on the sliding bubbles and nonsliding bubble

		D_d at liftoff, cm		End of the period of maximum bubble base											
							Contact angle								
Bubble type	Run no.	Measured	Predicted at $g_{z,m}$ (no sliding)	Bubble diameter D_m, cm	Base diameter $D_{b,m}$, cm	Velocity $V_{x,m}$, cm/s	$\beta_{a,m}$, deg	$\beta_{r,m}$, deg	$g_{z,m}$ (g/g_e)	$g_{x,m}$ (g/g_e)	$g_{y,m}$ (g/g_e)	F_b (N)	$F_{\mathrm{sh}-l}$ $(C_l=7.9)$, N	Sum $F_b+F_{\mathrm{sh}-l}$, N	$F-s$, N
Sliding	361	1.53	2.16	1.25	0.52	1.80	54	31	0.011	−0.009	0.003	1.1E−04	6.2E−04	7.3E−04	6.5E−04
	362	1.19	1.55	1.06	0.30	0.98	43	33	0.029	−0.009	0.004	1.7E−04	1.1E−04	2.9E−04	3.5E−04
	363	1.15	1.49	0.95	0.27	0.77	41	23	0.035	−0.009	0.004	1.5E−04	6.3E−05	2.1E−04	2.7E−04
	364	1.24	1.62	1.04	0.31	0.73	51	26	0.030	−0.010	0.003	1.7E−04	6.1E−05	2.3E−04	3.5E−04
	381	0.95	1.75	0.71	0.29	1.88	46	29	0.024	−0.023	−0.008	4.2E−05	2.2E−04	2.7E−04	3.3E−04
	382	0.74	0.98	0.60	0.18	1.04	44	22	0.049	−0.017	−0.014	5.2E−05	6.7E−05	1.2E−04	1.8E−04
	383	0.74	0.80	0.53	0.14	0.12	35	27	0.107	−0.007	−0.009	7.9E−05	1.4E−06	8.1E−05	1.3E−04
	386	1.31	2.03	1.10	0.47	2.25	42	29	0.010	−0.009	−0.008	6.8E−05	1.0E−03	1.1E−03	5.0E−04
	387	1.23	1.76	1.13	0.29	1.94	43	32	0.027	−0.009	0.001	1.9E−04	4.2E−04	6.1E−04	3.3E−04
	3817	1.52	2.89	1.32	0.47	1.67	40	26	0.010	0.005	0.008	1.1E−04	9.2E−04	1.0E−03	4.8E−04
	401	1.50	2.44	1.32	0.47	1.43	46	27	0.008	−0.007	0.000	9.0E−05	3.2E−04	4.1E−04	5.2E−04
	411	1.62	2.20	1.51	0.48	0.70	48	33	0.008	−0.007	0.001	1.3E−04	1.0E−04	2.4E−04	5.7E−04
	412	1.29	1.61	1.25	0.27	0.84	48	38	0.025	−0.006	0.002	2.4E−04	1.4E−04	3.8E−04	3.4E−04
	414	1.31	1.55	1.22	0.32	0.60	53	33	0.022	−0.008	0.001	2.0E−04	5.2E−05	2.5E−04	4.0E−04
	415	1.26	1.64	0.95	0.29	0.70	52	31	0.029	−0.008	0.004	1.2E−04	6.4E−05	1.9E−04	3.5E−04
	416	2.11	2.41	2.03	0.68	0.29	39	38	0.010	−0.003	0.002	4.1E−04	6.0E−05	4.7E−04	7.9E−04
	418	1.22	1.66	0.93	0.25	0.73	53	32	0.028	0.001	0.011	1.1E−04	1.2E−02	1.2E−02	3.1E−04
	752	1.21	1.89	1.13	0.34	1.40	45	29	0.016	−0.009	−0.004	1.2E−04	2.8E−04	3.9E−04	3.8E−04
	301	1.63	2.05	1.40	0.49	1.28	44	31	0.010	−0.008	−0.001	1.3E−04	3.0E−04	4.4E−04	5.5E−04
	341	1.62	2.57	1.43	0.46	1.05	41	39	0.009	−0.006	0.007	1.3E−04	4.5E−04	5.8E−04	5.5E−04
Nonsliding	——	——	——	——	——	——	β_a, deg, L	β_a, deg, R	——	——	——	——	——	——	——
	665	1.20	1.38	1.10	0.25	~0.0	39	40	0.040	0.016	−0.010	2.6E−04	——	——	2.9E−04
	670	1.25	1.23	1.17	0.25	~0.0	48	46	0.050	0.011	~0.000	4.0E−04	——	——	3.3E−04
	676	1.45	1.59	1.34	0.34	~0.0	35	36	0.030	0.002	~0.000	3.6E−04	——	——	3.6E−04
	677	1.70	1.85	1.60	0.40	~0.0	39	37	0.022	0.004	0.010	4.5E−04	——	——	4.5E−04
	680	1.40	1.38	1.19	0.30	~0.0	42	43	0.040	0.008	−0.010	3.3E−04	——	——	3.7E−04
	681	1.20	1.30	1.40	0.38	~0.0	46	44	0.045	0.006	−0.005	6.1E−04	——	——	5.0E−04
	683	1.90	1.94	1.47	0.28	~0.0	41	42	0.020	−0.002	~0.000	3.1E−04	——	——	3.4E−04
	685	1.15	1.08	1.03	0.26	~0.0	44	42	0.065	0.003	0.010	3.5E−04	——	——	3.2E−04
	688	1.20	1.30	1.06	0.26	~0.0	40	41	0.045	0.003	0.003	2.7E−04	——	——	3.0E−04
	689	1.62	1.59	1.59	0.43	~0.0	45	43	0.030	−0.015	0.050	5.9E−04	——	——	5.5E−04

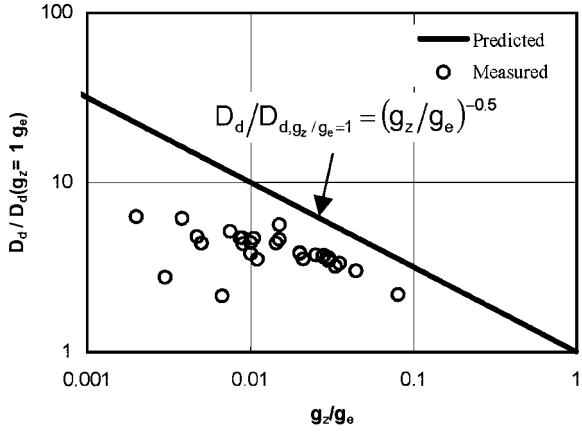

Fig. 18 Liftoff diameter of sliding bubbles as a function of gravity level.

behavior of sliding bubbles has also been observed in flow boiling.[17] The magnitude of the forces acting on the bubbles is estimated at the moment when bubble base starts to shrink and the bubble begins to lift off from the surface. This is the time when the downward force caused by surface tension is maximum. Thereafter, as the forces lifting the bubble off the surface exceed the downward force, the bubble base starts to shrink, and the net upward force acting on the bubble accentuates the bubble liftoff. The considered forces are surface tension force $F_s = \pi D\sigma \sin\bar{\beta}$ acting downward at the contact line between the bubble and the surface, buoyancy force $F_b = \pi D^3\ (\rho_l - \rho_v)g_z/6$, and shear-lift force $F_{\mathrm{sh}-l} = C_l\rho_l(\pi D^3/6)(V-U)|\mathrm{d}(V-U)/\mathrm{dz}| = C_l\rho_l(\pi/3)D^2V^2$. Here C_l is the shear lift coefficient, $(V-U)$ is the relative velocity of the bubble with respect to the bulk $(U \approx 0)$, $\mathrm{d}(V-U)/\mathrm{dz}$ corresponds to the vorticity term and is written as $V/(D/2)$. Both buoyancy and shear force act normal to the surface. This lift force appears to be of different in nature than the lift force calculated by Saffman[18] on a solid particle in a moving liquid and by Legendre and Magnaudet[19] for a bubble moving in a shear flow but is similar to that identified by Leighton and Acrivos[20] for a solid particle sitting on a solid and subjected to shear flow. The microgravity conditions provide a good means to explore the effect of the lift force on bubble liftoff, as the buoyancy force can be very small.

Thus, the force balance at the moment when bubble base begins to shrink is written as follows:

$$F_s = F_{\mathrm{sh}-l} + F_b$$

$$\pi D_{\mathrm{bm}}\sigma \sin\bar{\beta} = \pi D_m^3(\rho_l - \rho_v)g_z/6 + C_l\rho_l(\pi/3)D_m^2V^2 \quad (8)$$

where subscript m denotes the time at which bubble base begins to shrink and $\bar{\beta}$ the average contact angle taken as $(\beta_r + \beta_a)/2$, where β_r is in the upstream (receding) and β_a in downstream (advancing). As shown in the upper part of Table 1 and in Fig. 19a, for bubble liftoff at low gravity with sliding motion the force F_s is larger than F_b. Using the values of F_s and F_b and substituting for various parameters into the $F_{\mathrm{sh}-l}$ term, the shear lift coefficient is evaluated to be 7.9 from the present data set. This value of the coefficient is not considered to be universal as it will depend on the local velocity profile near the surface. No effort was made in this work to measure the velocity profile in the liquid. The shear lift force is seen to be comparable to the buoyancy force in most cases so as for the sum of $F_{\mathrm{sh}-l}$ and F_b to overcome the surface tension force and lift the bubble off from the surface (see Fig. 19b). In the lower part of Table 1, several cases without sliding are also listed; the magnitudes of F_s and F_b are close. This fact shows that Eq. (1) only describes a special case of the forces acting on the bubble at liftoff, that is, the case with the absence of bubble sliding motion.

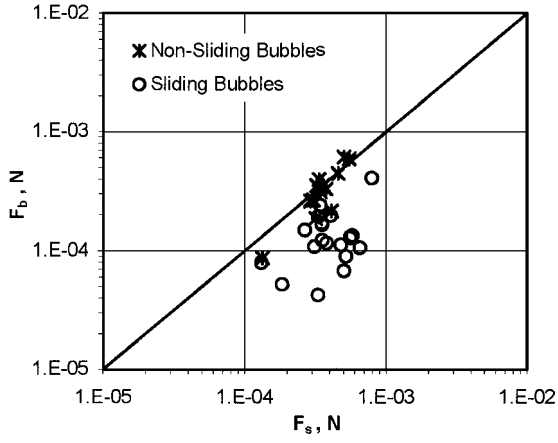

a) Comparison of surface tension force F_s and buoyancy force F_b

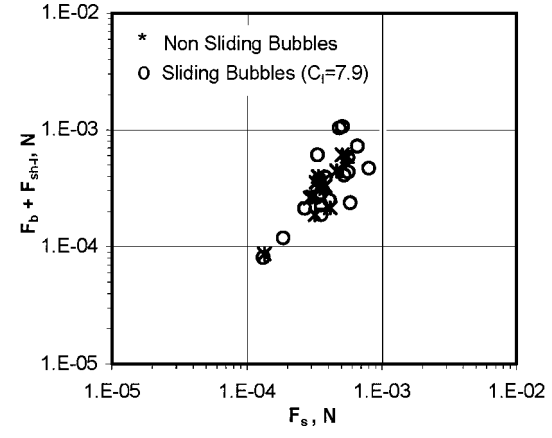

b) Comparison of surface tension force F_s and sum of buoyancy and shear lift forces $F_b + F_{sh-l}$

Fig. 19 Comparison of estimated forces acting on sliding bubbles and on nonsliding bubbles.

Conclusions

1) By making the artificial cavity in the polished silicon wafer, well-defined nucleation site has been achieved. This approach has allowed experimental study of dynamics of single vapor bubbles during nucleate boiling in the low-gravity conditions of KC-135 flight.

2) Larger bubble liftoff diameters and longer bubble growth periods than those at Earth normal gravity were measured. Bubble liftoff diameters as large as 20 mm were observed. Oblong spherical shapes with a varying base area on the heater surface was found to be the typical shape of the single bubbles.

3) Small subcooling in the liquid caused significantly prolonged bubble growth periods and reduced bubble growth rates.

4) When g_z dominated, the measured bubble liftoff diameters agree with the numerical predictions and confirm the fact that buoyancy and surface tension are the major forces during the bubble liftoff at low gravity. The results showed that the bubble liftoff diameter can be approximately related to the gravity level through the relation $D_d \propto (1/\sqrt{g})$ for single bubbles.

5) The experimental results of the bubble growth period before liftoff at low-gravity scale as $t_g/t_{g(g_z/g_e=1)} = (g_z/g_e)^{-1.05}$ in the range of $0.01\ g_e \le g_z \le 1.8\ g_e$, when g_z is dominant.

6) The existence of the acceleration components along the heater that were comparable to the component normal to the heater caused the bubbles to slide along the heater and acquired nonsymmetric shape. These in turn resulted in the bubble liftoff diameters to be smaller than those when gravity normal to the heater dominated. The shear-lift force caused by the relative velocity between the bubble and the surrounding liquid contributes to the early liftoff of the bubble.

Acknowledgment

This work received support from NASA under the Microgravity Fluid Physics Program.

References

[1]Keshock, E. G., and Siegel, R., "Forces Acting on Bubbles in Nucleate Boiling Under Normal and Reduced Gravity Conditions," NASA TN-D-2299, Aug. 1964.

[2]Siegel, R., and Keshock, E. G., "Effect of Reduced Gravity on Nucleate Bubble Dynamics in Water," *Journal of AIChE*, Vol. 10, No. 2, 1964, pp. 509–516.

[3]Ervin, J. S., Merte, H., Kellers, R. B., and Kirk, K., "Transient Boiling in Microgravity," *International Journal of Heat and Mass Transfer*, Vol. 35, No. 3, 1992, pp. 659–674.

[4]Ervin, J. S., and Merte, H., "Boiling Nucleation and Propagation in Microgravity," *Heat Transfer in Microgravity*, edited by C. T. Avedisian and V. A. Arpaci, HTD Vol. 269, American Society of Mechanical Engineers, New York, 1993, pp. 659–674.

[5]Merte, H., "Pool and Flow Boiling in Variable and Microgravity," *2nd Microgravity Fluid Physics Conference*, NASA John H. Glenn Research Center, Paper 33, June 1994.

[6]Lee, H. S., and Merte, H., "Pool Boiling Curve in Microgravity," *Journal of Thermophysics and Heat Transfer*, Vol. 11, No. 2, 1997, pp. 216–222.

[7]Straub, J., Zell, M., and Vogel, B., "Boiling Under Microgravity Conditions," *Proceedings of 1st European Symposium on FLUIDS IN SPACE*, ESA, SP-353, Ajaccio, France, 1992.

[8]Straub, J., "The Role of Surface Tension for Two-Phase Heat and Mass Transfer in the Absence of Gravity," *Experimental Thermal and Fluid Science*, Vol. 9, No. 3, 1994, pp. 253–273.

[9]Ohta, H., Kawaji, M., Azuma, H., Inoue, K., Kawasaki, K., Okada, S., Yoda, S., and Nakamura, T., "Heat Transfer in Nucleate Pool Boiling Under Microgravity Condition," *Proceedings of 11th International Heat Transfer Conference*, edited by J. S. Lee, Vol. 2, 1998, pp. 401–406.

[10]Kim, J., Benton, J. F., and Wisniewski, D., "Pool Boiling Heat Transfer on Small Heaters: Effects of Gravity and Subcooling Level," *Proceedings of Engineering Foundation Conference on Fluid, Thermal, Biological, and Material Sciences Conference II*, edited by S. S. Sadhal, Engineering Foundation, New York, 2001, pp. 379–389.

[11]Ma, Y., and Chung, J. N., "A Study of Bubble Dynamics in Reduced Gravity Forced-Convection Boiling," *International Journal of Heat and Mass Transfer*, Vol. 44, No. 2, 2001, pp. 399–415.

[12]Ramanujapu, N., and Dhir, V. K., "Dynamics of Contact Angle During Growth and Detachment of a Vapor Bubble at a Single Nucleation Site," *Proceedings of 5th ASME/JSME Joint Thermal Engineering Conference* [CD-ROM], American Society of Mechanical Engineers, San Diego, CA, 1999.

[13]Son, G., Dhir, V. K., and Ramanujapu, N., "Dynamics and Heat Transfer Associated with a Single Bubble During Nucleate Boiling on a Horizontal Surface," *Journal of Heat Transfer*, Vol. 121, No. 3, 1999, pp. 623–632.

[14]Singh, S., and Dhir, V. K., "Effect of Gravity, Wall Superheat and Liquid Subcooling on Bubble Dynamics During Nucleate Boiling," *Microgravity Fluid Physics and Heat Transfer*, edited by V. K. Dhir, Begell House, New York, 2000, pp. 106–113.

[15]Singh, S., "Effect of Gravity and Liquid Subcooling on Bubble Dynamics," M.S. Thesis, Mechanical and Aerospace Engineering Dept., Univ. of California, Los Angeles, Sept. 1999.

[16]Qiu, D. M., Dhir, V. K., Hasan, M. M., Chao, D., Neumann, E., Yee, G., and Birchenough, A., "Single Bubble Dynamics During Nucleate Boiling Under Low Gravity Conditions," *Microgravity Fluid Physics and Heat Transfer*, edited by V. K. Dhir, Begell House, New York, 2000, pp. 62–71.

[17]Maity, S., and Dhir, V. K., "An Experimental Study of Vapor Bubble Dynamics on Inclined Surfaces Subjected to Forced Flow Along the Surface," *Proceedings of 35th National Heat Transfer Conference* [CD-ROM], American Society of Mechanical Engineers, Anaheim, CA, 2001.

[18]Saffman, P. G., "The Lift on a Small Sphere in a Slow Shear Flow," *Journal of Fluid Mechanics*, Vol. 22, Pt. 2, 1965, pp. 385–400.

[19]Legendre, D., and Magnaudet, J., "A Note on the Lift Force on a Spherical Bubble or Drop in a Low Reynolds Number Shear Flow," *Physics of Fluids*, Vol. 9, No. 11, 1997, pp. 3572–3574.

[20]Leighton, D., and Acrivos, A., "The Lift on a Small Sphere Touching a Plane in the Presence of Simple Shear Flow," *Journal of Applied Mathematics and Physics*, Vol. 36, No. 1, 1985, pp. 174–178.